JOURNAL OF SPACECRAFT AND ROCKETS
Vol. 42, No. 1, January–February 2005

Numerical Simulation of Aeroacoustic Phenomena in a Solid Rocket Booster

P. Cosyn* and J. Vierendeels†
Ghent University, 9000 Ghent, Belgium
and
J. Anthoine‡
von Kármán Institute for Fluid Dynamics, 1640 Rhode-Saint-Genèse, Belgium

Flow instabilities in solid rocket boosters such as the Ariane 5 boosters could lead to pressure and thrust oscillations, which reduce the rocket motor performance and could damage the payload. Before any modification within the solid rocket boosters can be performed to eliminate the pressure oscillations, a good understanding of the fluid dynamic phenomena is needed. Because a complete analytical solution does not exist yet, experimental and numerical models need to be created as a platform for further investigation of these instabilities. We describe how a commercial computational-fluid-dynamics program (Fluent) can be used to simulate the aeroacoustic phenomena that exist in a solid rocket booster. The simulation is compared with experimental measurements of a 1/30-scale axisymmetric cold flow model of the Ariane 5 booster.

Nomenclature

a	=	speed of sound
C_p	=	specific heat at constant pressure
D	=	internal diameter of the model
D_p	=	diameter of the sintered particles
d	=	internal diameter of the inhibitor
e	=	thickness of the porous plate
f	=	frequency of the oscillation
i	=	acoustic mode number
L	=	total length
l	=	inhibitor-nozzle distance
M_0	=	mean Mach number
$\dot{m}$	=	mass flux
P_{rms}	=	rms pressure
P_s	=	static pressure
Pr	=	Prandtl number
p'	=	acoustic pressure
T	=	temperature of the flow
u	=	axial velocity
u'	=	acoustic velocity
v	=	radial velocity
γ	=	adiabatic constant
ΔP	=	pressure drop
μ	=	dynamic viscosity
ν	=	kinematic viscosity
ρ	=	density
ρ_m	=	mean density of the fluid flowing through the porous plate
σ	=	porosity of the plate

Presented as Paper 2003-3874 at the AIAA 33rd Fluid Dynamics Conference, Orlando, FL, 23–26 June 2003; received 4 July 2003; revision received 16 December 2003; accepted for publication 23 December 2003.

*Undergraduate Student; currently Ph.D. Candidate, Department of Flow, Heat and Combustion Mechanics, St.-Pietersnieuwstraat 41; peter.cosyn@ugent.be. Member AIAA.

†Professor, Department of Flow, Heat and Combustion Mechanics, St.-Pietersnieuwstraat 41; jan.vierendeels@ugent.be. Member AIAA.

‡Assistant Professor, Environmental and Applied Fluid Dynamics Department, Chausée de Waterloo 72; anthoine@vki.ac.be. Member AIAA.

Introduction

THE interior of a large solid rocket booster consists of a submerged nozzle and segmented propellant grains separated by inhibitors (Fig. 1). The inhibitor rings ensure thermal protection. During the combustion, the regression rate of the grains surface is faster than those of the inhibitor rings. The inhibitor rings form an obstacle in the burning flow. At the same time, the combustion of the propellant leads to the formation of a cavity around the nozzle. Vortical structures that appear at the inhibitor edge interact with the nozzle, which leads to pressure oscillations.[1,2] When the vortex shedding frequency reaches an acoustic mode of the motor chamber, a resonance effect can occur, and the amplitude of the pressure oscillations could increase drastically. The motor chamber could be seen as a closed tube for the acoustic field because of the sonic conditions at the nozzle throat. Pressure oscillations have been reported for the space shuttle redesigned solid rocket motor (SRM), the Titan-34D SRM, the Titan-IV solid rocket motor upgrade, and the Ariane 5 SRM.[3–7]

The pressure oscillations could originate from a vortex shedding at the inhibitor edge but also from flow instability. The perturbation in the propellant surface between two grains could trigger instability of the curved streamlines of the flow. The burning flow could be seen as a radial gas injection at constant velocity through a porous wall of a semi-infinite tube. The resulting flow is called the Taylor flow.[8] It can be shown that such a flow is linearly unstable.[9] The later instabilities are called surface vortex shedding; the instabilities formed at the inhibitor are denoted with the term obstacle vortex shedding or OVS. In the current numerical investigation only an axial injected flow model is simulated and compared with experiments executed on a scale model of the boosters. As a result, only OVS is investigated.

The presence of an obstacle downstream of the shedding point of the vortices can trigger the acoustic feedback when vortices interact with it.[10,11] In the case of the Ariane 5 booster, this second obstacle could be the nozzle. The process of acoustic instabilities creation could be described in the following five steps: 1) hydrodynamic instability of shear flow regions; 2) roll up, growth, and advection of vortices; 3) interaction of the vortices with the nozzle cavity and generation of an acoustic perturbation; 4) acoustic propagation from the downstream source; and 5) transfer of energy from the acoustic mode to the shear flow instability.

The generation of self-sustained sound resonance in a tube depends on the phase of the acoustic oscillation at which a vortex shed by the upstream obstacle reaches the downstream one.[12] This phase is determined by the time needed for a vortex to travel between the

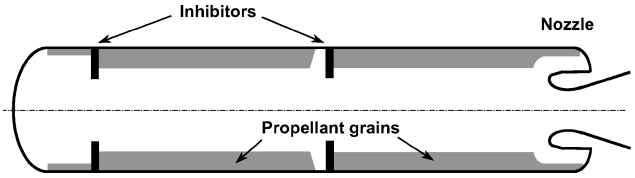

Fig. 1 Interior of a solid rocket booster.

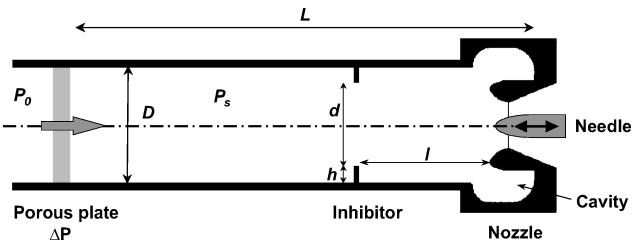

Fig. 2 Experimental setup.

inhibitor and the nozzle cavity entrance in the case of OVS. It is a function of the distance between the obstacles and the speed at which the vortex travels. To sustain an acoustic resonance effect, the vortex shedding has to be in phase with the acoustic properties of the tube. The acoustic modes of a closed tube can be derived analytically. Their frequencies are given by

$$f = f_{\mathrm{ac},i} = ia/2L$$

To validate the results of the numerical model, experiments have been conducted on a 1/30-scale axisymmetric cold flow model (Fig. 2). A cold-flow analysis is possible because the combustion has only a minor influence on the pressure peaks and frequencies. The experimental setup consists of a test section that includes a rigid inhibitor and a submerged nozzle with sonic conditions at the throat. The flow is created by an axial air injection. The internal diameter D of the segments, equal to 0.076 m, is based on the 1/30-scale similarity with the full-scale motor obtained by conserving the Mach number when 50% of the propellant is burnt. The total length L and the inhibitor parameters (d and l) can be modified. For comparison with the simulations, they will be constant with $d = 0.058$ m and $l = 0.07$ m. To simulate a change in Mach number that exists in the Ariane 5 solid rocket booster, a movable needle is used, placed in the nozzle throat. The experiments will be conducted at a constant Mach number for comparison with the numerical simulations. To minimize acoustic noise coming from the air supply in the test section, a porous plate is inserted at the forward end. This ensures an acoustic insulation of the test section by providing a high-pressure drop.[13] This pressure drop is of the order of magnitude of the static pressure in the test section. The acoustic pressure measurements are taken by means of PCB piezoelectric transducers from Piezotronics (model 106B50). A first probe is placed just downstream of the porous plate. A second one is mounted between the inhibitor and the nozzle, and a third one is placed in the cavity of the nozzle. The acoustic pressure is also measured just upstream the porous plate to verify the acoustic insulation. The velocity spectra are deduced from hot-wire experiments.[2] The acoustic pressure fluctuation data are acquired by means of a data-acquisition card controlled by Testpoint. The signals are filtered at 3 kHz and acquired at 7.5 kHz. For one measurement 8192 samples are saved. MATLAB® is used to determine the power spectrum of the pressure fluctuations.

Earlier Analytical and Experimental Research

An early interpretation of the phenomenon is from Flandro and Jacobs,[14] who linked the oscillations to the hydrodynamics instability of the sheared regions of the flow and to the coupled acoustical response of the motor. Most laboratory experiments were carried out with models operating with cold gases because combustion is believed to take a minor part in the instability mechanism. Cold-flow experiments in a pipe with one or two inhibitors were performed, for example by Culick and Magiawala,[15] Mettenleiter et al.,[16] and Anthoine.[2] Culick and Magiawala[15] showed that one inhibitor could not sustain the acoustic mode. An obstacle downstream was needed to provide the necessary feedback when the vortices interact with it.

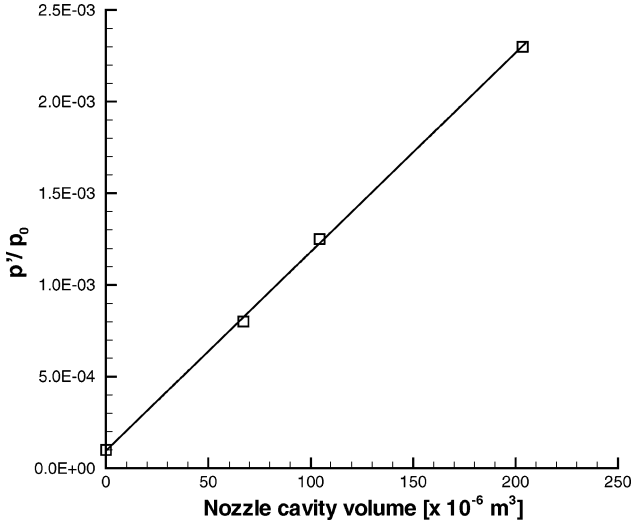

Fig. 3 Evolution of the maximum sound pressure level vs the nozzle cavity volume for excitation on the second acoustic mode at $M_0 = 0.08$, $l = 71$ mm, and $d = 58$ mm.

Couton et al.[17] conducted experiments in a two-dimensional channel with wall injection, obstacles simulating inhibitors, and a submerged nozzle. It was found that the channel resonance corresponding to the excitation of the first longitudinal modes and the amplification of the acoustic level depend on the injected mass flow rate. Other experiments indicated that the process is also controlled by the relative position of the vortex shedding position and the resonant mode. Brown et al.[3] and Dunlap and Brown[18] showed that the acoustic mode triggers vortex shedding more effectively at locations where the acoustic pressure features a node and acoustic velocity an antinode. In the case of OVS vortex shedding from a sharp edge, a large acoustical velocity at the vortex shedding point leads to a large initial absorption that can reduce the pressure peaks.[19] As a result, the optimal position for strong oscillation levels appears to be a compromise between initial absorption and strong feedback. For rigid diaphragms, the vortex-generation point should be located close to an acoustic velocity antinode to get large pressure oscillations.

It was found that the order of magnitude of the pulsation amplitude found in actual motors strongly depends on the design of the nozzle. In particular, when an integrated nozzle is used the pulsation increases linearly with the volume of the cavity formed around the nozzle inlet (Fig. 3).[1] Anthoine[2] showed that a simple analytical model based on vortex sound theory explains this linear dependence. The amplitude, however, was not correctly predicted. The experiments also indicated that sound is not necessarily produced by an actual impingement of the vortices with the nozzle but is rather a continuous process during the approach of the vortex with the cavity entrance. The sound produced during vortex ingestion by the nozzle might be less important.

Numerical Investigation

Fluent Code

Fluent version 6 was used for the simulations. The computational-fluid-dynamics (CFD) code uses cell-centered discretization schemes up to second order in space. The limited order of discretization in space could be a problem for acoustic computations, especially in the case of high-frequency acoustics. Because of the low rate of dissipation of high-order terms in an acoustic field in comparison with the convective properties of a flow, it was believed that at least a fourth-order discretization scheme was needed to resolve the acoustic field correctly. Of course, it also depends on the density of the grid. In this investigation a second-order upwind scheme has been used because a fourth-order algorithm was not included in the CFD code. An explicit four-stage Runge–Kutta time

stepping of the Jameson type was used.[20] However, a second-order spatial scheme will be sufficient if the grid density is chosen carefully. A Courant–Friedrich–Lewy (CFL) number of 1 was imposed. This resulted in a time step of about 4×10^{-7} s with the used grid.

Methodology of the Numerical Approach

The methodology followed to perform the numerical simulation is summarized in Fig. 4.

The two-dimensional axisymmetric Navier–Stokes equations are solved under the assumption of a laminar flow. The grid dependency was checked first. The acoustic spectra at the forward end were computed for three grids with different densities (14,000, 24,000, and 60,000 cells). The amplitude and frequency of the pressure and velocity peaks were compared. The investigations showed that 14,000 cells were sufficient to resolve the acoustic phenomena within the frequency range of the excited acoustic modes.

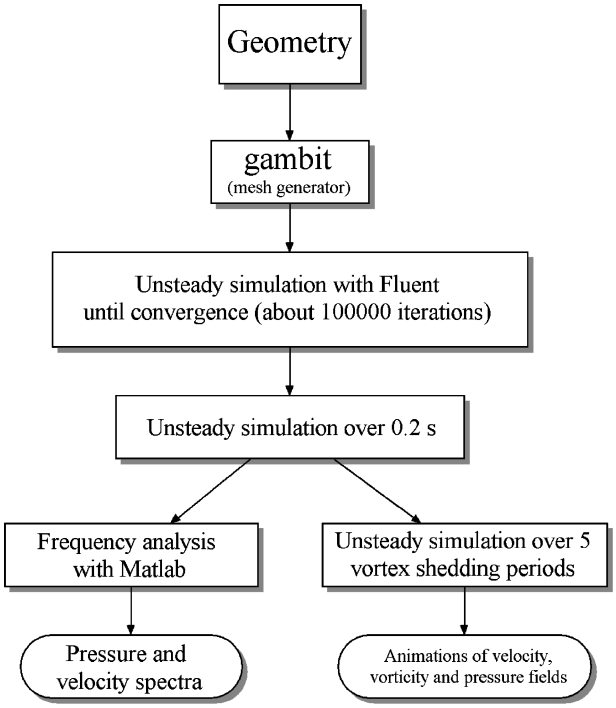

Fig. 4 Methodology.

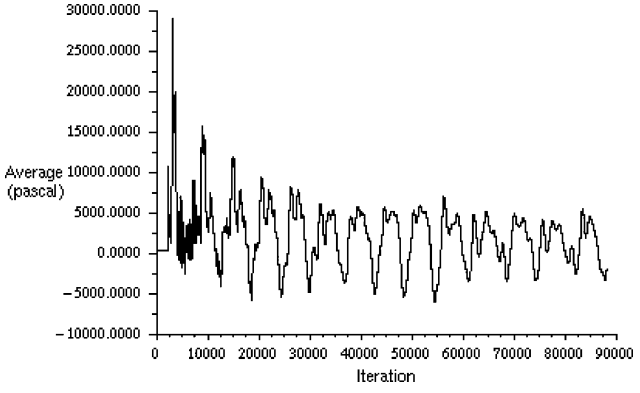

Fig. 5 Convergence of the pressure at the inlet.

To compute the sound pressure level, a converged unsteady pressure signal is necessary. Therefore a preliminary simulation is executed, and the static pressure at the inlet is monitored. After about 10^5 iterations the pressure amplitude does not drop anymore, and the solution can be considered as being converged (Fig. 5).

In a next step, the simulation is performed for a total time of 0.2 s. With the used grid and a CFL number of 1, this corresponds to about 5×10^5 iterations. A physical time of 0.2 s corresponds to a frequency resolution of 5 Hz. This is a minimum requirement to get a useful frequency resolution of the pressure and velocity signals. The pressure and velocity signals are monitored in 27 virtual sensors. Figure 6 shows the positions of those sensors. The positions of sensors 1, 2, and 3 correspond to the positions of the PCB sensors in the experimental setup. Sensor 4 is placed on the nozzle head, 5 and 6 are positioned in the throat of the nozzle, 7 measures the pressure at the inhibitor axis, and 8 measures the pressure signal at the inlet on the axis of the booster. The other virtual sensors measure the velocity fluctuations along the radius between inhibitor and nozzle. They are used to get the velocity profiles of u and v along the radius. Those are compared with the hot-wire experiments.

The frequency spectra of the time signals are computed with a MATLAB® program. The rms values of the pressure are divided by the static pressure to make the pressure spectra dimensionless.

To visualize the behavior of the flowfield, an unsteady simulation of five vortex-shedding periods is performed, and for every period 20 images of the static pressure, the velocity magnitude, and the vorticity are saved and fit in to an animation of those flow variables.

Grid and Boundary Conditions

The geometry and the mesh were generated with gambit (version 1.3), a preprocessor of Fluent. The geometry could be created in two dimensions because the problem has an axisymmetric geometry. The throat of the nozzle has a diameter of 0.03 m, and this corresponds with a Mach number M_0 of 0.09 in the case of sonic conditions at the throat section. The Mach number M_0 is the Mach number of the flow upstream the inhibitor. The diameter of the booster, the nozzle-inhibitor distance, and the dimensions of the inhibitor are as described earlier. The thickness of the inhibitor is 3 mm, and the total length of the booster is 0.393 m. This is the distance between the inlet and the top of the most distant point of the cavity along the symmetry axis. It corresponds to the total length of the experimental setup.

A structured grid with quadrilateral cells is used with a fine resolution around the inhibitor and the vortex path. The numerical domain was divided into blocks to generate the grid. A part of the geometry at the nozzle and inhibitor is shown in Fig. 7. The grid dependency is checked as described before. To obtain the grids with 24,000 and 60,000 cells, the density of the grid was changed uniformly by altering the number of grid points on the edges of the blocks.

The axial injected flow is cold air, which is inert, single phase, and at γ constant. The physical properties of the flow are $T = 285$ K,

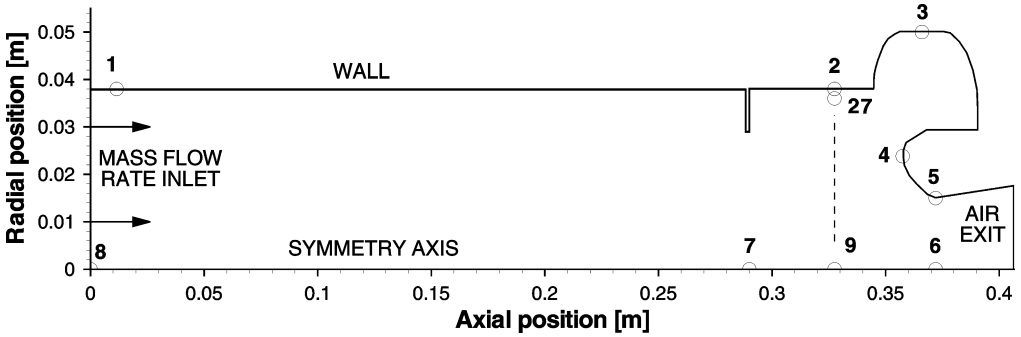

Fig. 6 Position of the virtual sensors.

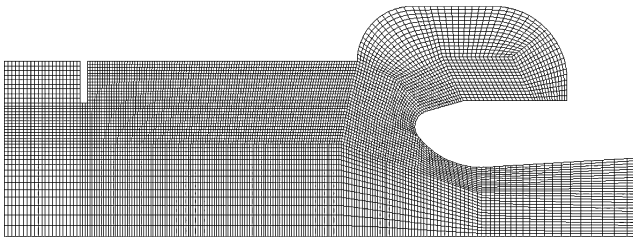

Fig. 7 Mesh at the inhibitor and nozzle.

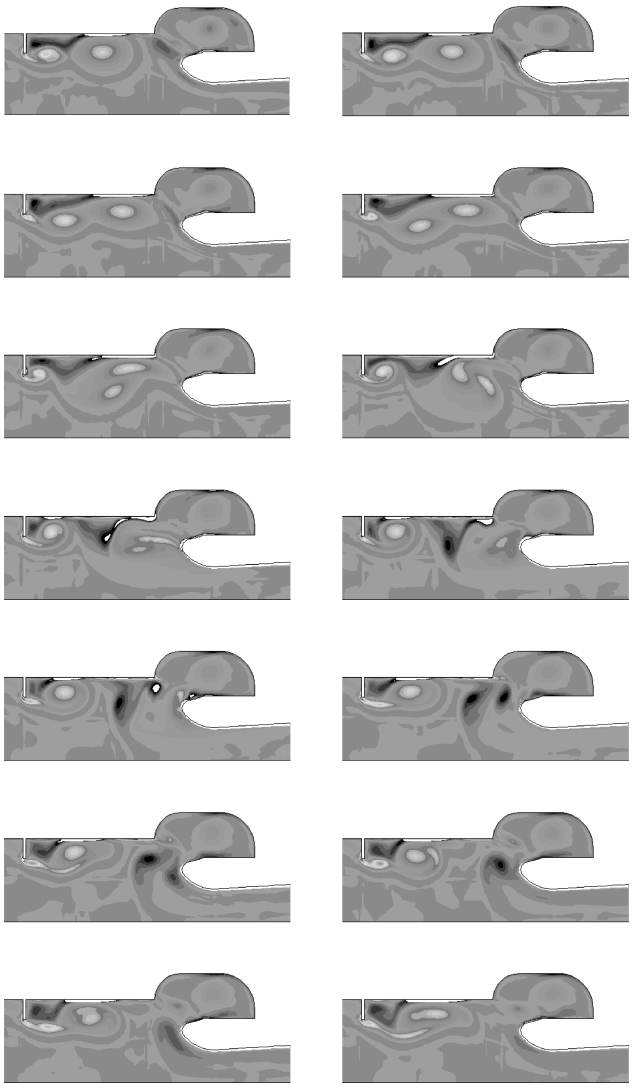

Fig. 8 Vorticity evolution. A time step of 2×10^{-4} s exists between every frame.

$Cp = 1006$ J/(kg · K), $\gamma = 1.4$, $Pr = 0.71$, and $\mu = 1.7894 \times 10^{-5}$ Pa.s. The cold air is considered to be an ideal gas.

The static pressure P_s is chosen to allow comparison to the experimental data ($P_s = 178$ kPa). The boundary conditions at the inlet of the booster consist of an axial injected mass flux $\dot{m}$, which is equal to 66.3 kg · s^{-1} · m^{-2} for a static pressure of 178 kPa. The boundary condition at the exit of the nozzle corresponds to a far away pressure of 10 kPa to obtain a sonic condition at the nozzle throat. The bottom line of the numerical domain is the axis of symmetry. The other boundaries are walls at 285 K with a no-slip condition.

Numerical Results

Vortex Shedding

Figure 8 gives the time evolution of the vorticity magnitude in the internal of the booster. The vorticity is defined as the curl of the velocity vector. Between every picture there is a time step of 2×10^{-4} s. The vorticity magnitude is limited to [−20,000, 60,000 s^{-1}] to have a good visibility of the vortex structures in the flow. The white spots are mostly concentrated at the walls and indicate shear layers where the vorticity magnitude is outside the limited interval. The figure shows that vortex shedding occurs at the inhibitor. The shear layer at the inhibitor is transported downstream, curls up, and sheds because the layer becomes unstable. The vortex is transported towards the nozzle and collides with the nozzle head. A part of the vortex disappears through the nozzle throat, and another part enters the cavity. This later part forms a static vortex in the cavity, which is continuously energized by new vortices. Another effect that happens is the pairing of two vortices. Because of this pairing, it is possible that the vortex shedding frequency does not correspond to an acoustic mode. This happens at certain Mach number, and experiments show that this can be seen as a drop in excited acoustic mode. The shedding frequency of the vortex structures is about 820 Hz.

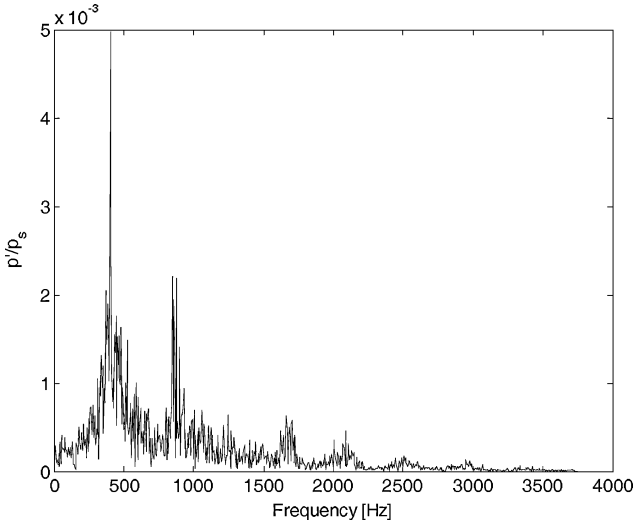

Fig. 9 Pressure spectrum of sensor 9.

Pressure and Velocity Spectra

Figure 9 shows a typical pressure spectrum. The peaks in the pressure spectrum correspond to the excitation of acoustic and hydrodynamic modes as described next. The hydrodynamic peak reflects the vortex-shedding frequency. The other peaks correspond to the excitation of the acoustic modes. The figure gives the pressure spectrum of virtual sensor 9. The left-hand part of Fig. 10 gives the pressure spectra for two other virtual sensors (1 and 3). The pressure spectrum at the inlet presents four peaks around 405, 850, 1255, and 1700 Hz. Those correspond to the excitation of the first four longitudinal acoustic modes. The first mode peak is the most energetic one with a maximum sound pressure level of about 2300 Pa, corresponding to $P_{\text{rms}}/P_s = 0.9 \times 10^{-2}$. The four modes are also visible in the other pressure spectra, but the amplitude differs. This is a result of the spatial form of the acoustic modes. Virtual sensors 1 and 3 are located closely to an antinode of the acoustic modes, the peaks are higher then those at virtual sensor 9. The higher noise level of the spectra of the sensors downstream the inhibitor is an effect of the irregular velocity fluctuations caused by the jet flow and the vortex structures. Figure 11 gives the spectra of the velocity components u and v of sensor 25, which is located in the path of the vortices. The effect of the hydrodynamic peak is more pronounced because the magnitudes of the acoustic velocity fluctuations are an order of magnitude less strong. This follows directly out of the velocity and pressure distributions of standing waves in a closed tube. For the first longitudinal acoustic mode with $p' = 2300$ Pa, the expected longitudinal acoustic velocity component would be

$$u' = p'/(\rho \cdot a) \approx 3.3 \text{ m/s}$$

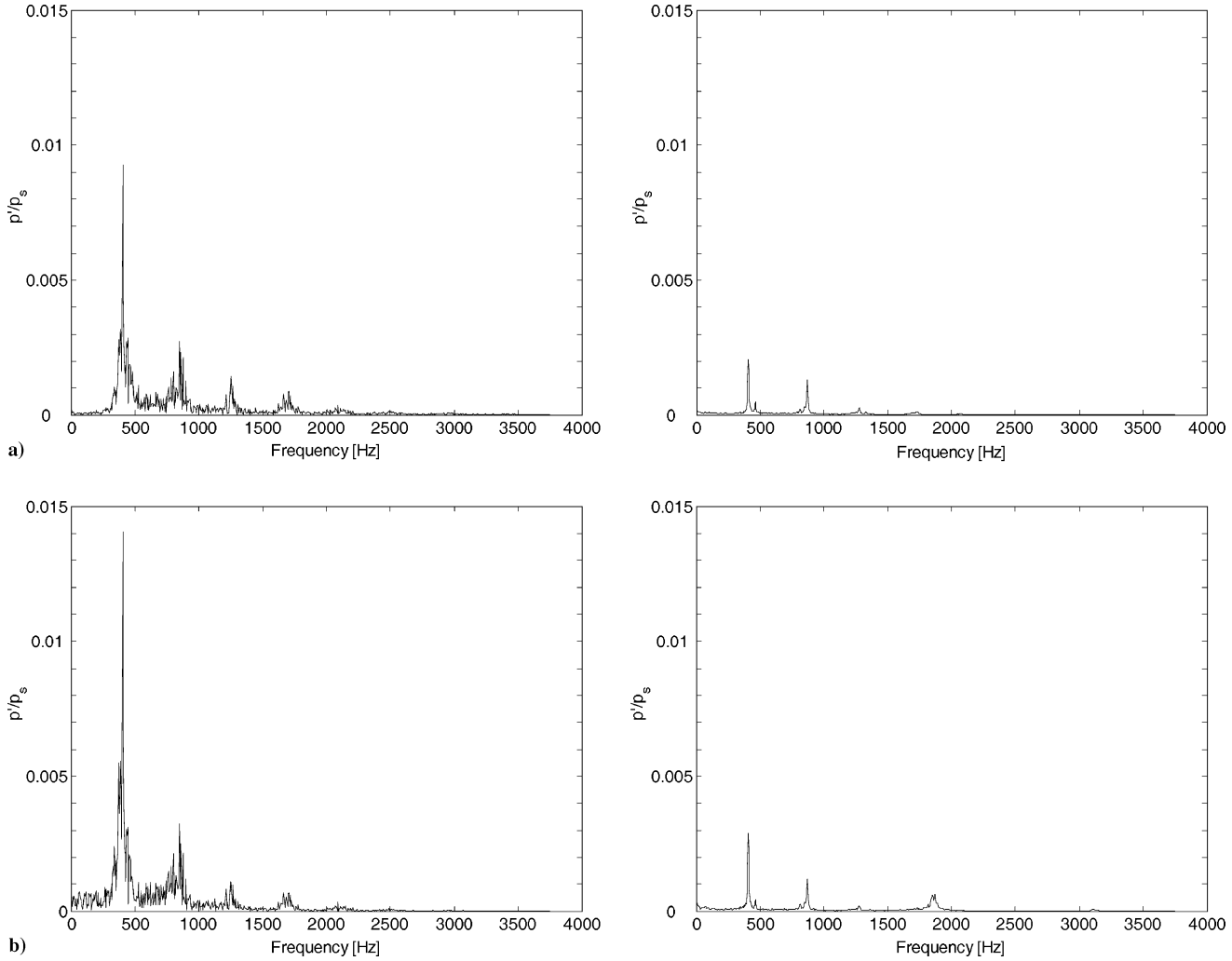

Fig. 10 Presssure spectrum of virtual sensors a) 1 and b) 3. They are compared with the experimental pressure spectra of the PCBs at the inlet and cavity.

Comparison with the Experiments

The acoustic pressure spectra of the virtual sensors 1 and 3 are compared with the experimental results. The reference pressure of the experimental results is measured with the static-pressure probe (type Validyne) just downstream the porous plate. The reference pressure of the simulated pressure spectra is the static mean pressure at the virtual sensor 1. This pressure is about 178,000 Pa and is about the same as the pressure measured by the Validyne. Figure 10 shows the spectra for the virtual sensors 1 and 3 and compares them with the experiments. The frequencies of the pressure peaks are very well simulated. However, the magnitudes are overestimated with a factor 5. The relative difference between the first and second mode peak can be explained by a slight difference in Mach number between experiments and the simulation. The pairing effect of the vortices excites the first acoustic mode. However, this pairing does not happen every time, and as a result the second peak can be increased. The Mach-number dependency of this pairing effect can be seen on Fig. 12, which gives an experimental result with a change in Mach number. It contains the data of the PCB at the inlet. The crosses indicate the position of the most excited mode, and the line indicates the relative pressure magnitude of the most excited mode. It is clear from the figure that the pairing effect happens in a relative short interval. If the Mach number is a little less than 0.09, then the second mode is more excited than the first mode. There are different possible causes to explain the difference of a factor 5 between the first mode of the experiments and the simulation.

A first cause could be the inlet condition. The mass flow rate is a function of the pressure drop through the porous plate. The pressure upstream of the porous plate does not change, but the pressure downstream the porous plate changes because of the pressure fluctuations of the acoustic modes. This can be described with the Ergun equation (see Refs. 21 and 22), which gives the pressure drop as a function of the mass flux $\dot{m}$, the thickness of the plate e, the porosity σ, the diameter of the sintered particles D_p, and fluid parameters like the adiabatic constant γ and the kinematic viscosity ν:

$$\Delta P/e = [(1-\sigma)/\sigma^3]\left\{150\left[(1-\sigma)\nu\Big/D_p^2\right]\dot{m}_i + 1.75(1/D_p\rho_m)\dot{m}_i^2\right\}$$

This is computed from the arithmetic average of the pressure on both sides of the plate:

$$\rho_m = \gamma\left[(P_s + \Delta P/2)\Big/a^2\right]$$

This equation can be implemented in Fluent for example by using user-defined functions. Anthoine[2] showed that the pressure peaks can be halved by using a better inlet condition. A second cause could be dissipative effect of the vortical structures because of turbulence and two- to three-dimensional transition of the instabilities. This does not happen in a laminar axisymmetric simulation. Turbulences are introduced in the flow because of irregularities at the porous plate. The Reynolds number based on the internal diameter of the booster is about 5×10^5, which is a lot more than the Reynolds number needed for a turbulent flow which is about 10^4 for a pipe flow. Figure 13 provides a comparison of the computed mean velocity profiles with those obtained experimentally using particle-image-velocimetry technique (PIV). The profiles are compared at

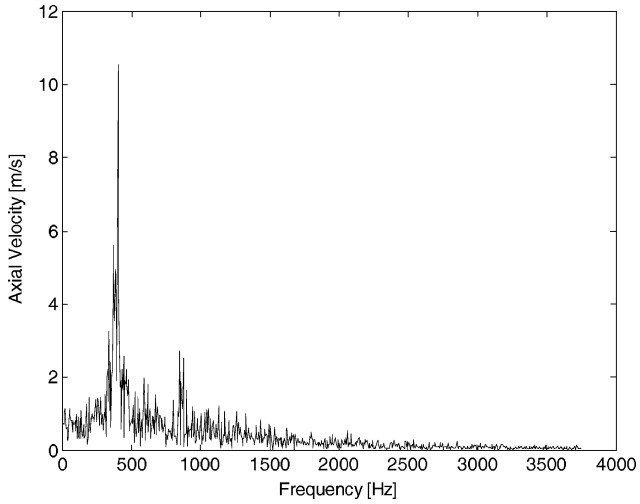

a) Axial

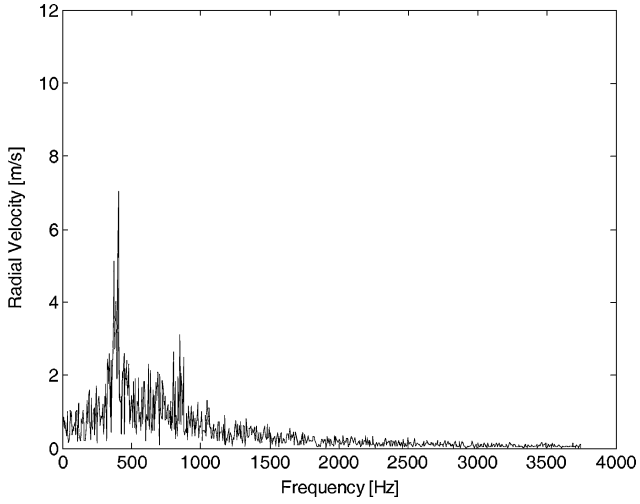

b) Radial

Fig. 11 Velocity spectrum for virtual sensor 25.

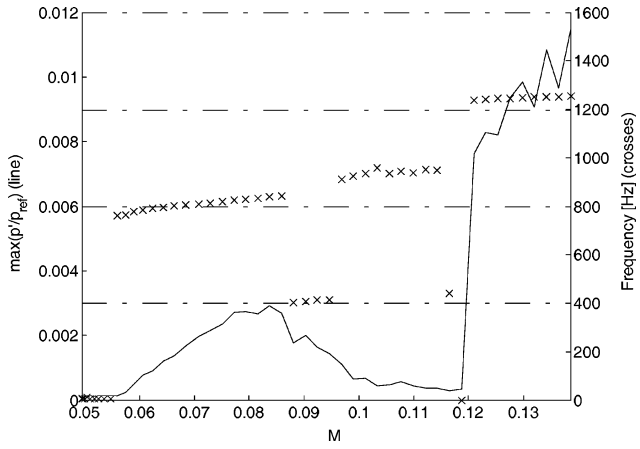

Fig. 12 Mach-number dependency of the acoustic velocity spectrum (sensor 1).

an axial distance of 0.33 m from the porous plate, so downstream the inhibitor. The PIV measurements were performed in a cold-flow model at 1/15-scale (Ref. 23). The axial and radial mean velocity profiles are close even if some deviations are observed at the limits of the recirculation bubble, where the velocity gradients are important. The hot-wire anemometry technique has also been used to measure mean velocity profile in the cold-flow model at 1/30-scale used for pressure measurements (Fig. 2). Figure 14 shows a comparison between Fluent, PIV, and hot wire. Because the hot wire is only sensitive to the flow amplitude and cannot detect the flow direction, only the mean velocity amplitude is plotted. The numerical and PIV results are then analyzed to obtain velocity amplitudes. We see a good comparison between the three sets of data. Close to the wall, the hot-wire results are overestimated because this technique is sensitive to fluctuations. These fluctuations are important close to the wall. Although Fluent and the PIV technique will see fluctuations as positive and negative quantities around zero as mean value, the hot wire will see only positive amplitudes resulting in a positive and overestimated mean velocity.

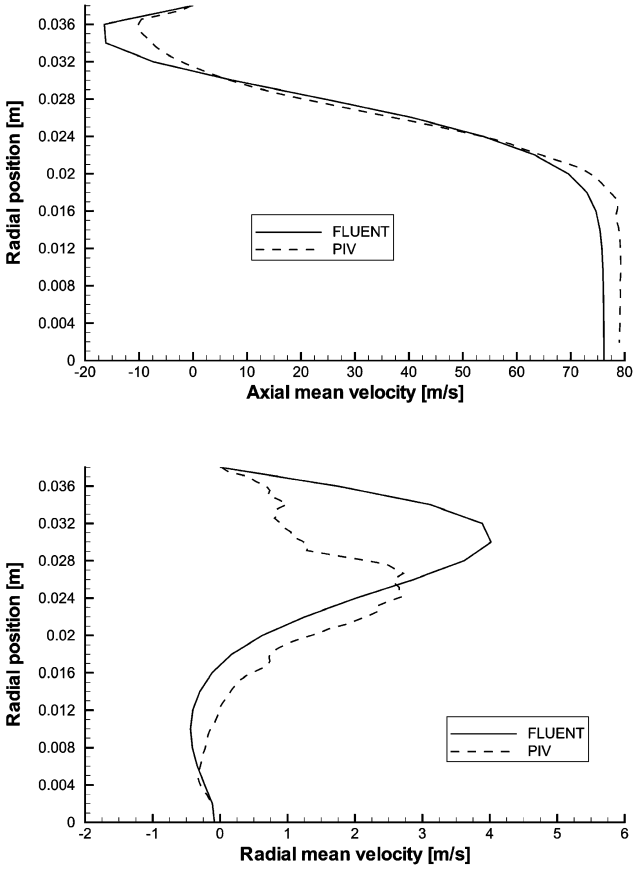

Fig. 13 Comparison of velocity profiles between numerical simulations and cold-flow experiments.

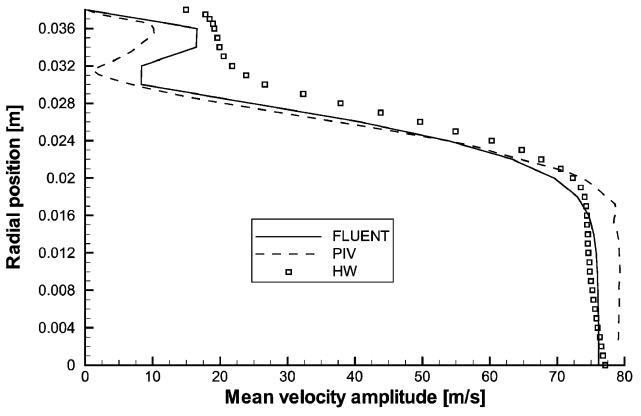

Fig. 14 Comparison of velocity amplitude profiles between numerical simulations and cold-flow experiments.

Conclusions

A numerical simulation of the internal of a solid rocket booster has been performed with a commercial computational-fluid-dynamics

code, Fluent. The acoustic phenomena are observed and compared with experiments of a 1/30-scale axisymmetric cold flow model of the Ariane-5 SRM with purely axial injected flow.

A laminar approach with constant wall injection is investigated. A second-order spatial algorithm was sufficient to capture the flowfield. Comparison with the experiments shows that the flow field is well predicted and that the acoustic frequencies of the pressure peaks are in good agreement with the experiments. However, the pressure peaks are overestimated with a factor five. A more realistic model will be needed to get a better prediction of the pressure peaks. A better inlet condition and the use of a turbulence model can reduce the pressure peaks significantly.

Acknowledgments

This research has been done at the von Kármán Institute and Ghent University. The authors thank Koenraad Janssens for his help during the present research.

References

[1]Anthoine, J., Buchlin, J.-M., and Hirschberg, A., "Effect of Nozzle Cavity on Resonance in Large SRM: Theoretical Modeling," *Journal of Propulsion and Power*, Vol. 18, No. 2, 2002, pp. 304–311.

[2]Anthoine, J., "Experimental and Numerical Study of Aeroacoustic Phenomena in Large Solid Propellant Boosters," Ph.D. Dissertation, Univ. Libre de Bruxelles, Brussels, Oct. 2000.

[3]Brown, R. S., Dunlap, R., Young, S. W., and Waugh, R. C., "Vortex Shedding as a Source of Acoustic Energy in Segmented Solid Rockets," *Journal of Spacecraft and Rockets*, Vol. 18, No. 4, 1981, pp. 312–319.

[4]Dotson, K. W., Koshigoe, S., and Pace, K. K., "Vortex Shedding in a Large Solid-Rocket Motor Without Inhibitors at the Segmented Interfaces," *Journal of Propulsion and Power*, Vol. 13, No. 2, 1997, pp. 197–206.

[5]Mason, D. R., Folkman, S. L., and Behring, M., "Thrust Oscillations of the Space Shuttle Solid-Rocket Booster Motor During Static Tests," AIAA Paper 79-1138, June 1979.

[6]Blomshield, F. S., and Mathes, H. B., "Pressure Oscillations in Post-Challenger Space Shuttle Redesigned Solid-Rocket Motors," *Journal of Propulsion and Power*, Vol. 9, No. 2, 1993, pp. 217–221.

[7]Scippa, S., Pascal, P., and Zanier, F., "Ariane-5 MPS: Chamber Pressure Oscillations Full-Scale Firings Results Analysis and Further Studies," AIAA Paper 94-3068, June 1994.

[8]Taylor, G. I., "Fluid Flow in Regions Bounded by Porous Surfaces," *Proceedings of the Royal Society of London, Series A: Mathematical and Physical Sciences*, Vol. 234, No. 119, 1956, pp. 456–475.

[9]Varapaev, V. N., and Yagodkin, V. I., "Flow Stability in a Channel with Porous Walls," *Izvestiya Akademii Nauk SSSR, Meckanika Zhidkostii Gaza [Fluid Dynamics]*, Vol. 4, No. 5, 1969, pp. 91–95.

[10]Flatau, A., and Van Moorhem, W., "Vortex Shedding Induced Sound Inside a Cold-Flow Simulation of Segmented Chamber," *Journal of Propulsion and Power*, Vol. 19, No. 2, 2003, pp. 287–296.

[11]Schachenmann, A., and Rockwell, D., "Self-Sustained Oscillations of Turbulent Pipe Flow Terminated by an Axisymmetric Cavity," *Journal of Sound and Vibrations*, Vol. 73, No. 1, 1980, pp. 61–72.

[12]Hourigan, K., Welsh, M. C., Thompson, M. C., and Stokes, A. N., "Aerodynamic Sources of Acoustic Resonance in a Duct with Baffles," *Journal of Fluids and Structures*, Vol. 4, 1990, pp. 345–370.

[13]Anthoine, J., and Olivari, D., "Cold Flow Simulation of Vortex Induced Oscillations in a Model of Solid Propellant Boosters," AIAA Paper 99-1826, May 1999.

[14]Flandro, G. A., and Jacobs, H. R., "Vortex-Generated Sound in Cavities," AIAA Paper 73-1014, Oct. 1973.

[15]Culick, F. E. C., and Magiawala, K., "Excitation of Acoustic Modes in a Chamber by Vortex Shedding," *Journal of Sound and Vibration*, Vol. 64, No. 3, 1979, pp. 455–457.

[16]Mettenleiter, M., Haile, E., and Candel, S., "Adaptive Control of Aeroacoustic Instabilities," *Journal of Sound and Vibration*, Vol. 230, No. 4, 2000, pp. 761–781.

[17]Couton, D., Plourde, F., and Doan, S., "Analysis of Energy Transfers of a Sheared Flow Generated by Wall Injection," *Experiments in Fluids*, Vol. 26, No. 3, 1999, pp. 222–232.

[18]Dunlap, R., and Brown, R. S., "Exploratory Experiments on Acoustic Oscillation Driven by Periodic Vortex Shedding," *AIAA Journal*, Vol. 19, No. 3, 1981, pp. 408, 409.

[19]Hirschberg, A., Bruggeman, J. C., Wijnands, A. P. J., and Smits, N., "The Whistler Nozzle and Horn as Aero-Acoustic Sound Sources in Pipe Systems," *Acoustica*, Vol. 68, No. 2, 1989, pp. 157–160.

[20]Jameson, A., Schmidt, W., and Turkel, E., "Numerical Solution of the Euler Equations by Finite Volume Methods Using Runge–Kutta Time-Stepping Schemes," AIAA Paper 81-1259, June 1981.

[21]Ergun, S., "Flow Through Packed Columns," *Chemical Engineering Progress*, Vol. 48, 1952, pp. 89–94.

[22]Bird, R. B., Stewart, W. E., and Lightfoot, E. N., *Transport Phenomena*, Wiley, New York, 1960, p. 200.

[23]Anthoine, J., Mettenleiter, M., Repellin, O., Buchlin, J.-M., and Candel, S., "Influence of Adaptive Control on Vortex-Driven Instabilities in a Scaled Model of Solid Propellant Motors," *Journal of Sound and Vibration*, Vol. 262, No. 5, 2003, pp. 1009–1248.

T. Lin
Associate Editor